

## The C<sub>4</sub>H<sub>6</sub><sup>+</sup> Potential Energy Surface. 2. The Reaction of Ethylene Radical Cation with Acetylene

Vojtěch Hrouda, Petr Čárský,\* Marek Ingr, and Zdenek Chval†

J. Heyrovský Institute of Physical Chemistry, Academy of Sciences of the Czech Republic, Dolejškova 3, 182 23 Prague 8, Czech Republic

G. Narahari Sastry‡ and Thomas Bally\*

Institut de Chimie Physique, Université de Fribourg, Pérolles, 1700 Fribourg, Switzerland

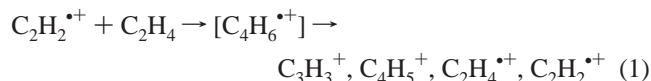
Received: June 11, 1998; In Final Form: August 24, 1998

The reaction of the ethylene radical cation (Et<sup>•+</sup>) with acetylene (Ac) to form stable C<sub>4</sub>H<sub>6</sub><sup>•+</sup> intermediates and the subsequent fragmentation of these to C<sub>3</sub>H<sub>3</sub><sup>+</sup> + CH<sub>3</sub><sup>•</sup> or to C<sub>4</sub>H<sub>5</sub><sup>+</sup> + H<sup>•</sup> have been studied by the UMP2, RMP2, and B3LYP methods with the 6-31G\* basis set, as well as by single-point calculations at the RCCSD-(T)/cc-pVTZ level of theory. The aim of this study was to identify all stationary points that might be relevant to explain the course of the observed reactions. According to their stability to dissociation, we distinguish three classes of C<sub>4</sub>H<sub>6</sub><sup>•+</sup> structures: weakly bonded complexes, structures of medium stability, and tightly bonded complexes. Methylcyclopropene radical cation seems to be the most likely ultimate precursor for the formation of the observed fragmentation products.

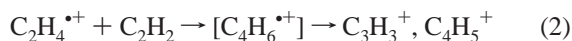
### 1. Introduction

The knowledge of potential energy surfaces (PESs) of polyatomic ions is of basic importance for interpreting experiments both on the bimolecular reaction dynamics of ion–molecule processes and on the dynamics of unimolecular decomposition of polyatomic state-selected ions. In the former, scattering studies of bimolecular ion–molecule processes often reveal the formation of intermediate complexes. Angular distributions of products may be related to the structures and dynamics of the dissociating intermediate. In the latter case, the energetics and the decomposition of ions prepared from parent molecules are investigated by the photoelectron–photoion coincidence (PEPICO) method; “experimental PESs” (energetics of minima and barriers) obtained from the resulting data can be greatly refined by theoretical calculations. C<sub>4</sub>H<sub>6</sub> has been subjected to both types of experimental investigations.<sup>1</sup>

This study has been stimulated by crossed-beam scattering experiments on the dynamics of formation of various products in the system



studied by Herman and his collaborators.<sup>2</sup> Analogous products were observed for the “charge inverted” reaction



The reactions in both systems appear to proceed through common intermediates on the way to form the products. From scattering diagrams and from the angular and product translational energy distributions, the formation of an intermediate

C<sub>4</sub>H<sub>6</sub><sup>•+</sup> with a mean lifetime > 5 × 10<sup>-12</sup> was inferred.<sup>2,3</sup> For the reaction channels leading to C<sub>3</sub>H<sub>3</sub><sup>+</sup> + CH<sub>3</sub><sup>•</sup> and to C<sub>4</sub>H<sub>5</sub><sup>+</sup> + H<sup>•</sup>, angular distributions indicated<sup>2</sup> that the critical configuration of the dissociating intermediate is consistent with the structure of methylcyclopropene radical cation (MCPE).

Obviously, ab initio calculations may be very helpful in this case by yielding additional evidence on the structure and energy of intermediates and transition states, especially on the way to various dissociation products. By its size, the C<sub>4</sub>H<sub>6</sub><sup>•+</sup> system is amenable to treatments by levels of the theory that provide results of sufficient accuracy for this purpose. We decided, therefore, to undertake an ab initio study on the C<sub>4</sub>H<sub>6</sub><sup>•+</sup> potential energy surface.

Most previous studies on C<sub>4</sub>H<sub>6</sub><sup>•+</sup> focused on the ring opening of the methylenecyclopropane radical cation (MCPA)<sup>4</sup> or the cyclobutene radical cation (CB).<sup>5,6</sup> Our own results on the latter reaction were presented separately,<sup>7</sup> whereas the present paper is intended to focus on the pathways for C<sub>4</sub>H<sub>6</sub><sup>•+</sup> association and fragmentation processes. Before the completion of this study, another paper with a similar scope was published by Keister et al.<sup>8</sup> They reported on the kinetics and mechanism of methyl loss from 1,3-butadiene (BD) and MCPE studied by threshold photoelectron–photoion coincidence time-of-flight mass spectrometry (TPEPICO), ab initio UMP2/6-311G\*\* calculations, and RRKM statistical theory. In earlier papers, Baer and collaborators<sup>1,9,10</sup> had described photoionization studies involving other C<sub>4</sub>H<sub>6</sub> isomers, 1,2-butadiene (methylallene, MA), 1-butyne (BTY), 2-butyne (dimethylacetylene, DA), and cyclobutene (CB). They concluded that the corresponding radical cations formed by photoionization rearranged to a common precursor prior to dissociation to C<sub>3</sub>H<sub>3</sub><sup>+</sup> + CH<sub>3</sub><sup>•</sup> and that the transition states for isomerizations among the different C<sub>4</sub>H<sub>6</sub><sup>•+</sup> species lie below the dissociation limit. Preuninger and Farrar<sup>11</sup> arrived at the same conclusion in their photofragmentation study of BD, MA, CB, and MCPE. The absence of photodissociation products from BTY and DA, reported by Preuninger and Farrar,<sup>11</sup> was explained later by Bunn and Baer.<sup>10</sup>

\* Present address: Faculty of Biology, University of South Bohemia, České Budejovice, Czech Republic.

† Present address: Department of Chemistry, University of Pondicherry, 605014 Pondicherry, India.

Dissociation of the BD radical cation has also been investigated by Dannacher et al.<sup>12,13</sup> and by Russell et al.<sup>14,15</sup>

The most comprehensive study on the  $C_4H_6^{*+}$  PES by ab initio calculations is contained in the above-mentioned recent paper by Keister et al.<sup>8</sup> (other work concerned mainly the ring opening of  $CB^+$ , which is treated in detail in our other paper<sup>7</sup>). However, this study was based entirely on the UMP2 methodology, which is known to be prone to artifacts due to UHF spin contamination,<sup>16</sup> especially also in the case of weakly bound ion–molecule complexes.<sup>17</sup> We therefore decided to pursue our investigation of the  $C_4H_6^{*+}$  PES using a wider range of computational methods, hoping that this would uncover and eliminate possible artifacts of the previously used methods, such as they arise by spin contamination or symmetry breaking. Although we strived to arrive at a comprehensive picture of the  $C_4H_6^+$  PES (insofar as it is relevant with regard to the mechanism of processes 1 and 2 above), no claim of completeness is made.

## 2. Computational Methods

All structures were optimized by the standard UHF, UMP2, and B3LYP methods, as implemented in the Gaussian 94 program.<sup>18</sup> In cases of ROHF convergence problems, optimizations were carried out with Gamess/US.<sup>19</sup> Stationary points were characterized by harmonic frequency calculations at all the above levels. From the available variants of the restricted open-shell MP2 method,<sup>20</sup> we selected that<sup>21,22</sup> implemented, along with analytical gradients, in the Cadpac<sup>23</sup> and Aces2 codes.<sup>24</sup> All geometry optimizations were carried out with the standard 6-31G\* basis set,<sup>25</sup> and in the MP2 calculations, all electrons were correlated. At the optimized UMP2 and B3LYP geometries, we also performed single-point RCCSD(T) calculations, by the method of Knowles et al.<sup>26</sup> as implemented in the Molpro program package.<sup>27</sup> These were done with Dunning's correlation-consistent triple- $\zeta$  (cc-pVTZ) basis set,<sup>28</sup> which can be expected to give accurate energies at this level of theory.

In addition to Hessian calculations, all transition-state structures were tested by intrinsic reaction coordinate (IRC) calculations<sup>29</sup> to identify the minima they interconnect. Differences in zero-point energies ( $\Delta ZPE$ ) for the evaluation of  $\Delta E_0 = \Delta E + \Delta ZPE$  were taken from frequencies calculated at the level used for geometry optimization, except for the cases of RMP2 and RCCSD(T)/cc-pVTZ energies, which were corrected on the basis of B3LYP frequencies, if the respective stationary point existed, and by UMP2 frequencies in other cases.

As with any calculation on processes of the type  $A + B \rightarrow AB$ , where AB is a loosely bonded complex, incompleteness of the basis set forces one to consider the effects of basis set superposition error (BSSE). For some relevant cases, we calculated this error at the ROHF and RMP2 levels by a variant of the Boys–Bernardi method,<sup>30</sup> which takes into account the bond relaxation energy.<sup>31</sup> For the distonic  $^+CHCHCH_2CH_2^{\bullet}$  radical cation, which may also be viewed as a  $(C_2H_2 \cdots C_2H_4)^+$  complex cation, the BSSE is 1.2 and 5.5 kcal/mol at the ROHF and RMP2 levels, respectively. For the  $(C_3H_3^+ \cdots CH_3^{\bullet})$  complex, the corresponding numbers are 0.6 and 1.0 kcal/mol. We decided, therefore, not to correct the energies of loosely bonded complexes for BSSE, because it brings about only a minor change in the overall energy diagram and does not alter any of our conclusions with regard to the reaction path of processes 1 and 2.

To show that the single-determinant reference wave functions are adequate to provide a correct description of the molecular

characteristics, CASSCF single-point calculations using seven active electrons in eight orbitals were carried out on all UMP2 stationary points. In all cases, the ground-state reference determinant contributed  $\geq 90\%$  (typically by 93%) and no individual excited state contributed more than 3.9% (typically  $\leq 2.0\%$ ) to the CASSCF wave function. The expectation value  $\langle S^2 \rangle$  in the unrestricted Hartree–Fock (UHF) determinants was always less than 0.78 in the B3LYP calculations, whereas in the UHF reference wave function used for UMP2 it showed significant deviations from 0.75, especially at transition states, where it sometimes exceeded 0.95.

## 3. Results and Discussion

Before going into details below, we should mention that the energetics of all our calculations will refer to the reaction of the ethylene radical cation ( $Et^+$ ) with acetylene (Ac), although the original experiments<sup>2</sup> were done with  $Ac^+ + Et$ , which lie 21 kcal/mol higher in energy.<sup>32</sup> However, this only affects the total energy of the  $C_4H_6^{*+}$  system in these experiments and not the shape of the underlying PES. Under conditions of excess energy dissipation, charge transfer from  $Ac^+$  to Et would occur before anything else, thus bringing the system to the starting point of our calculations.

**3.1. Weakly Bonded Complexes.** Building on our previous experience with the  $Et + Et^+$  reaction<sup>17</sup> and the  $Ac + Ac^+$  reaction,<sup>33</sup> we engaged in a systematic characterization of four possible types of weakly bonded complexes. At first sight, a planar  $2s + 2s$  type complex of  $C_{2v}$  symmetry (PIC) would seem to constitute a favorable bonding arrangement as it provides optimal overlap between the  $\pi$  MOs of the two constituent species. Although this results in a bonding of 17 kcal/mol (see Table 1), it turns out not to be optimal, as in the previous cases of  $(Et \cdots Et)^+$  and  $(Ac \cdots Ac)^+$ , presumably because steric repulsion prohibits a sufficiently close approach.

The PIC structure turns out to be a transition state<sup>34</sup> interconnecting two automeric perpendicular complexes of  $C_{2v}$  symmetry (PpC), similar to the situation found in  $(Ac)_2^{*+}$ .<sup>33</sup> The perpendicular conformation seems to allow for better bonding, as PpC lies about 3 kcal/mol below PIC (see Table 1). At the SCF levels, PpC is a saddle point ( $-115 \text{ cm}^{-1}$  at ROHF,  $-127 \text{ cm}^{-1}$  at UHF) which, according to IRC calculations, represents a transition state for the interconversion of two three-membered-ring complexes of  $C_s$  symmetry (TC) where one end of the ethylene moiety bonds to the  $\pi$  system of acetylene.

At B3LYP, this stationary point has *two* imaginary modes, one of which ( $-96 \text{ cm}^{-1}$ ) is also associated with TC automerization, whereas the other one ( $-95 \text{ cm}^{-1}$ ) leads to an alternative three-membered-ring complex where one acetylene terminus binds to the ethylene  $\pi$  system. However, bonding in this latter species, which may be viewed as a cyclopropylcarbene radical cation (CC), is much stronger, and we will, therefore, return to this pivotal intermediate in the following section on tightly bound structures.

By UMP2, PpC is a minimum, but this is so shallow (separated from TC by a barrier of only 0.02 kcal/mol, associated with a transition state TS1 with an imaginary frequency of  $-88 \text{ cm}^{-1}$ ) that this should probably be regarded as an artifact. The vibrational mode connecting PpC with CC is also positive at UMP2 and thus gives rise to another transition state, TS2. This lies, however, 5 kcal/mol above PpC and turns out to be a second-order saddle point<sup>35</sup> whose other imaginary mode ( $-77 \text{ cm}^{-1}$ ) leads to the “linear complex” discussed below.

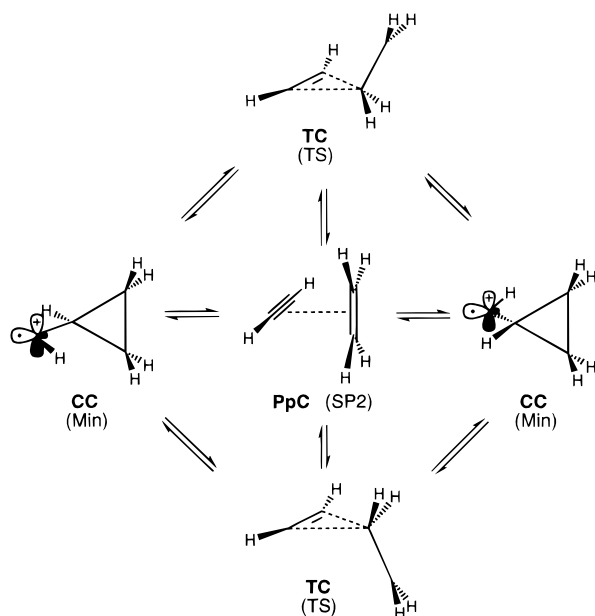
TC lies 0.5–1 kcal/mol lower in energy than PpC at all levels. By ROHF and UMP2, TC is a minimum, whereas UHF and

**TABLE 1: Energies and 0 K Enthalpies (kcal/mol) Relative to Ac + Et<sup>•+</sup> of Weakly Bonded C<sub>4</sub>H<sub>6</sub><sup>•+</sup> Complexes and Associated Transition Structures**

structure <sup>a</sup>	B3LYP/6-31G*		RMP2/6-31G <sup>*b</sup>		UMP2/6-31G*		RCCSD(T)/cc-pVTZ <sup>c</sup>	
	$\Delta E$	$\Delta E_0$	$\Delta E$	$\Delta E_0$	$\Delta E$	$\Delta E_0$	$\Delta E$	$\Delta E_0$
PIC <sup>d</sup>	-25.32	-23.46	-19.05	-15.28	-18.46	-14.69	-16.67	-14.81
PpC <sup>d</sup>	-27.21	-25.19	-22.22	-18.49	-21.58	-17.85	-19.55	-17.53
TC <sup>e</sup>	-27.54	-25.32	-22.54	-19.09	-21.94	-18.49	-20.53	-18.30
LC	<i>f</i>		-29.58	-23.54	-21.15	-15.11	-23.17	-17.13
TS1: PpC → TC	<i>g</i>		<i>g</i>		-21.56	-17.98	-20.57	-16.99
TS2: PpC → CC	<i>g</i>		<i>g</i>		-16.34	-11.83	-21.88	-17.37
TS3: LC → CC	<i>g</i>		<i>g</i>		-20.68	-14.38	-24.07	-17.77
TS4: TC → LC	<i>g</i>		<i>g</i>		-20.57	-16.64	-21.30	-17.37
CC <sup>j</sup>	-41.06	-36.15	-40.69	-34.08	-39.36	-32.75	-37.04	-32.13
Ac <sup>•+</sup> + Et	19.93	20.87	22.31	23.57	22.32	23.58	19.22	20.16
Ac + Et <sup>•+</sup>								
<i>E</i> <sup>h</sup>	-155.541 20		-155.002 72		-155.002 72		-155.242 15	
ZPE <sup>i</sup>	47.55		47.73		47.73		47.55	

<sup>a</sup> For UMP2 and B3LYP optimized structures, see Figure 2; structures TSx are transition states at UMP2 and B3LYP; all other species are minima, except where indicated otherwise. <sup>b</sup> For RMP2, vibrational analysis was not performed;  $\Delta$ ZPE taken from vibrational analysis at UMP2 level. <sup>c</sup> Single-point calculations at B3LYP (when these are available) or UMP2 geometries;  $\Delta$ ZPE taken from B3LYP and UMP2 vibrational analysis, respectively. <sup>d</sup> Transition state at UMP2, second-order saddle point at B3LYP. <sup>e</sup> Transition state at B3LYP. <sup>f</sup> Not found at B3LYP. <sup>g</sup> Not found at B3LYP and RMP2. <sup>h</sup> Total energies in hartrees. <sup>i</sup> Zero point energies in kcal/mol.

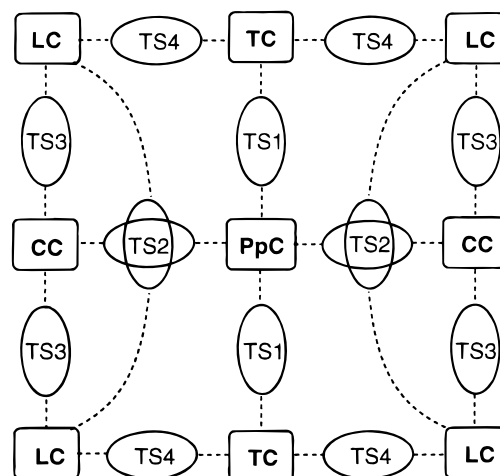
### SCHEME 1: Connection of Loosely Bound Complexes, PpC and TC, to CC on the B3LYP Potential Energy Surface



B3LYP IRC calculations show it to be a transition state for CC automerization. This completes the picture at the B3LYP level (cf. Scheme 1), but all other methods predict the existence of another loosely bound species on the C<sub>4</sub>H<sub>6</sub><sup>•+</sup> PES, the above-mentioned linear complex, <sup>•</sup>CH<sub>2</sub>CH<sub>2</sub>CHCH<sup>•+</sup> (LC),<sup>36</sup> which is of the type which corresponds to the most stable complexes in (Et)<sub>2</sub><sup>•+</sup><sup>17</sup> and (Ac)<sub>2</sub><sup>•+</sup>.<sup>33</sup>

LC is more strongly bound than TC at the RMP2<sup>37</sup> and RCCSD(T) levels, but at UMP2, this species is penalized by the comparatively high degree of spin contamination of the UHF wave function ( $\langle S^2 \rangle = 0.805$ ). Nevertheless, UMP2 predicts transition states TS3 (-476 cm<sup>-1</sup>) and TS4 (-169 cm<sup>-1</sup>), which separate LC from CC and TC, respectively (cf. Scheme 2).<sup>38</sup> However, on inclusion of zero-point energies, TS1 disappears, and at the RCCSD(T) level, the activation energies associated with all four transition states discussed above disappear. Thus, the minima predicted by UMP2 seem to be artifacts created by the tendency of transition states to have higher UHF spin

### SCHEME 2: Connection of Loosely Bound Complexes, PpC, TC, and LC, to CC on the UMP2 Potential Energy Surface<sup>a</sup>



<sup>a</sup> Structures, see Figure 2. Squares represent potential energy minima, ovals saddle points (crossed ovals: second-order saddle points).

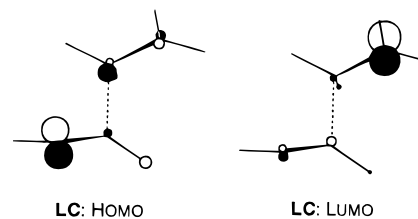


**Figure 1.** Frontier molecular orbitals of complex LC.

contamination than equilibrium structures. Consequently, Scheme 1 probably represents a PES that is closer to reality than Scheme 2.

As in (Et)<sub>2</sub><sup>•+</sup> and (Ac)<sub>2</sub><sup>•+</sup>, LC adopts a twisted geometry (dihedral angle of 116°),<sup>39</sup> but in contrast to the above symmetric complexes, the inherent dissymmetry of the (Et<sup>••</sup>Ac)<sup>•+</sup> complex results in a localization of spin and charge on opposite ends of the molecule. This feature expresses itself clearly in the shape of the HOMO and LUMO shown in Figure 1, which demonstrates also that the HOMO no longer has an antibonding component along the central bond so that this can assume a

shorter length. This situation is reminiscent of the species LC2 in  $(\text{Ac})_2^{*+}$ , which lies, however, higher in energy than the corresponding delocalized state, LC1.<sup>33</sup>

Interestingly, the charge in LC is localized on the acetylene moiety, although the ethyl radical (IP = 8.12 eV)<sup>40</sup> is easier to ionize than the vinyl radical (IP = 8.25 eV).<sup>41</sup> The reason for this apparent contradiction is that the ethyl cation is substantially stabilized by hyperconjugation with the methyl group ( $\text{CH}_3^+$  is 1.7 eV harder to ionize<sup>42</sup> than  $\text{H}_3\text{CCH}_2^+$ ); whereas the FMOs in Figure 1 indicate that this stabilizing interaction is virtually absent in LC. In view of this, one should compare the ionization energy of  $\text{CH}_3^+$  to that of the vinyl radical (1.6 eV in favor of the latter) to explain the distribution of spin and charge in LC. In fact, CASSCF(7,8) calculations (at the UMP2 geometry) predict that the state with exchanged spin and charge lies 54 kcal/mol above the ground state of LC. However, the separation of spin and charge in the excited state is less distinct than in the ground state.

A methodologically interesting observation on LC is, that it does not exist as a stationary point on the B3LYP surface (any attempt to locate a stationary point corresponding to LC leads to spontaneous collapse to CC). We had observed previously the reluctance of DFT models to separate spin and charge in radical cations,<sup>33,43</sup> and the same feature appears to be responsible for the inability of B3LYP to model LC: inspection of the spin and charge distribution from a B3LYP calculation (at the UMP2 geometry) shows that both are nearly fully delocalized, a fact which expresses itself in the shape of the B3LYP Kohn–Sham HOMO of LC. Thus, the localization of spin and charge which seems to be required in the present case to form a minimum on the PES cannot be modeled with DFT.

Summing up our results on weakly bonded  $(\text{Et}\cdots\text{Ac})^+$  complexes in Figure 2 and Table 1, we note that none of them seems to represent a stable species. In  $(\text{Et})_2^{*+}$  and  $(\text{Ac})_2^{*+}$ , the linear complexes were potential energy minima, but the separation of spin and charge in the corresponding  $(\text{Et}\cdots\text{Ac})^+$  species leads to the disappearance of the barriers separating it from more tightly bound species.

**3.2. Tightly Bound Structures.** *3.2.1. Spontaneous Relaxation to CB.* As we have shown above, in the vicinity of the weakly bonded complexes, the surface of the potential energy is relatively flat and only feebly structured with shallow minima and low-lying transition states. Consequently, the number and nature of these stationary points varies for different methods. Of the various channels connecting the weak complexes with tightly bound  $\text{C}_4\text{H}_6^{*+}$  species, the one leading to CC turns out to represent by far the most favorable pathway, with an activation barrier of less than 1 kcal/mol (see Table 1 and Scheme 1). This situation is closely analogous to that encountered in  $\text{C}_4\text{H}_4^{*+}$ ,<sup>33</sup> where we also found a nearly activationless collapse of a linear complex to a CC-type structure.

As in  $\text{C}_4\text{H}_4^{*+}$ , CC represents a shallow minimum of  $C_s$  symmetry with spin and charge located at the formally divalent carbon atom at UMP2 and B3LYP. At the SCF levels, the  $C_s$  form of CC is a very flat saddle point, with negative frequencies of  $-34$  and  $-134$   $\text{cm}^{-1}$ , respectively, connecting two slightly distorted automeric minima of  $C_1$  symmetry. However, this distortion probably represents a case of artificial symmetry breaking that disappears when correlation is included and is therefore not relevant for practical reasons.<sup>44</sup> However, CC must also be considered as a fleeting intermediate, because it collapses to CB via transition state TS5 (Figure 3) with a UMP2 barrier of only 0.6 kcal/mol, which furthermore disappears at the

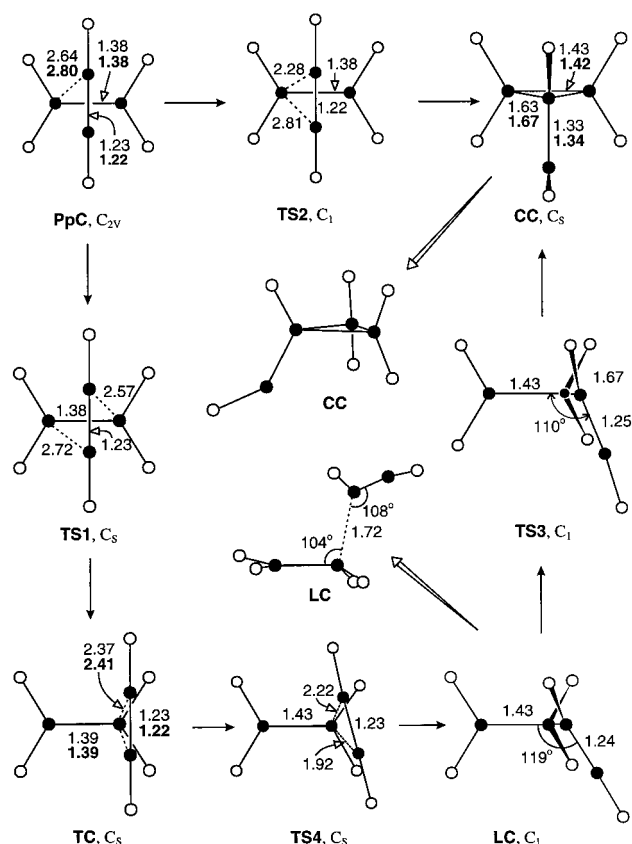


**Figure 2.** Interconnection and structures of stationary points in the loosely bound region of the  $[\text{C}_2\text{H}_4\cdots\text{C}_2\text{H}_2]^+$  potential energy surface by UMP2 (normal face) and B3LYP (bold face). Bond lengths in Å, angles in deg. Center: alternate views of LC and CC.

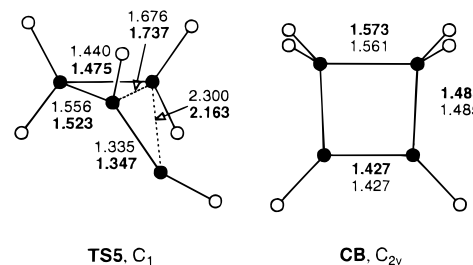


**Figure 3.** Structures of CB and the transition state, TS5, connecting it to CC (normal, UMP2; bold, B3LYP; bond lengths in Å, angles in deg).

CCSD(T)/cc-pVTZ level (cf. Table 2). Hence, as in  $\text{C}_4\text{H}_4^{*+}$ , there is no relevant obstacle for the activationless collapse of  $\text{Et}^{*+} + \text{Ac}$  to the four-membered-ring structure, CB.

The rearrangements among the stable CB valence isomers are described in some detail in a separate publication.<sup>7</sup> However, to put the subsequently discussed H shifts into perspective, we recall three important transition states, TS6 and TS7, for the conversion of CB to the radical cations of *cis*- and *trans*-BD, respectively, and TS8 for interconversion of the two BD rotamers (for pictorial representations, see ref 7). Finally, we should also mention that for stable  $\text{C}_4\text{H}_6^{*+}$  isomers as well as for some fragmentation products discussed in this study, the experimental enthalpy differences to  $\text{Et}^{*+} + \text{Ac}$  are available, and they are in very good agreement with the calculated RCCSD(T)  $\Delta H$  values (see Table 3).

*3.2.2. Alternative Rearrangement Paths of Weakly Bonded Complexes.* We have found two other reaction paths leading from the weakly bonded complexes to stable  $\text{C}_4\text{H}_6^{*+}$  isomers. The first of these represents a [1,3] hydrogen shift in LC, which

TABLE 2: Energies and 0 K Enthalpies (in kcal/mol) Relative to Ac + Et<sup>•+</sup> of Tightly Bonded C<sub>4</sub>H<sub>6</sub><sup>•+</sup> Structures

structure <sup>a</sup>	B3LYP/6-31G*		RMP2/6-31G <sup>b</sup>		UMP2/6-31G*		RCCSD(T)/cc-pVTZ <sup>c</sup>	
	$\Delta E$	$\Delta E_0$	$\Delta E$	$\Delta E_0$	$\Delta E$	$\Delta E_0$	$\Delta E$	$\Delta E_0$
BU1	-39.02	-37.52	-29.09	-26.87	-28.83	-26.61	-30.61	-29.10
MCPE	-41.16	-38.22	-40.12	-35.89	-37.64	-33.42	-34.83	-31.89
BTY	-44.38	-40.12	-37.93	-31.67	-37.26	-31.00	-37.22	-32.96
CC	-41.06	-36.15	-40.69	-34.08	-39.36	-32.75	-37.04	-32.13
PRC	-50.96	-46.66	-44.26	-38.70	-39.98	-34.42	-43.05	-38.74
BU2	-49.68	-46.25	-44.14	-38.64	-41.60	-36.09	-43.22	-39.79
MCPA	-55.17	-51.00	-47.40	-42.14	-47.36	-42.11	-45.68	-41.50
CB	-63.08	-58.16	-57.76	-51.76	-57.60	-51.60	-55.49	-50.58
MA	-69.97	-66.14	-60.24	-54.34	-56.90	-51.00	-59.52	-55.69
<i>cis</i> -BD	-84.05	-78.33	-78.57	-71.84	-72.45	-65.72	-74.14	-68.41
<i>trans</i> -BD	-87.72	-81.98	-82.59	-75.86	-76.67	-69.94	-77.62	-71.88
TS5: CC → CB	-39.99	-34.90	-40.95	-34.43	-38.77	-32.25	-37.23	-32.15
TS6: CB → <i>cis</i> -BD	-44.20	-40.08	<i>d</i>		-35.86	-30.16	-37.24	-33.12
TS7: CB → <i>trans</i> -BD	-40.89	-37.36	<i>d</i>		-27.82	-16.30	-36.30	-32.76
TS8: <i>cis</i> -BD → <i>trans</i> -BD	<i>e</i>		-49.55	-41.72	-49.06	-41.23	-49.28	-41.45
TS9: LC → <i>trans</i> -BD	<i>e</i>		-11.67	-9.13	-11.44	-8.90	-12.78	-10.24
TS10: BU1 → LC	<i>e</i>		-11.43	-9.21	-11.39	-9.16	-15.22	-12.99
TS11: BU1 → <i>cis</i> -BD	-36.96	-35.50	-28.75	-25.47	-27.90	-24.62	-31.73	-30.27
TS12: BU1 → BU2	-34.99	-34.03	<i>d</i>		-27.70	-25.93	-29.29	-28.32
TS13: BU2 → MCPA	-49.65	-46.34	<i>d</i>		-41.39	-36.11	-43.15	-39.84
TS14: BU1 → MA	-34.89	-33.33	<i>d</i>		-19.87	-16.49	-25.62	-24.06
TS15: MA → <i>trans</i> -BD	-26.20	-24.04	<i>d</i>		-14.39	-10.75	-19.57	-17.41
TS16: CC → BTY	-8.97	-6.04	-6.20	-1.22	-1.00	-3.98	-7.63	-4.69
TS17: CC → MCPE	-14.92	-12.58	-10.62	-7.00	-10.55	-6.94	-10.18	-7.84
TS18: <i>cis</i> -BD → PRC	-31.87	-30.38	-24.44	-21.07	-19.01	-15.65	-25.83	-24.00
TS19: PRC → MCPE	-40.15	-37.30	-38.79	-34.33	-31.46	-27.00	-34.88	-32.03

<sup>a</sup> For UMP2 and B3LYP optimized structures, see Figures 3–8; structures TSx are transition states; all other species are minima, unless indicated otherwise. <sup>b,c</sup> See footnotes in Table 1. <sup>d</sup> Not found at RMP2. <sup>e</sup> Not found at B3LYP.

TABLE 3: Experimental and Calculated 298 K Enthalpies (kcal/mol) of C<sub>4</sub>H<sub>6</sub><sup>•+</sup> Isomers Relative to Et<sup>•+</sup> + Ac<sup>a</sup>

	<i>trans</i> -BD	CB	MCPA	MCPE	C <sub>4</sub> H <sub>5</sub> <sup>+</sup> + H <sup>•</sup>	cyclopropenium + CH <sub>3</sub> <sup>•</sup>	propargyl + CH <sub>3</sub> <sup>•</sup>
expt	-73.7 ± 0.3 <sup>b</sup>	-54.1 ± 1.0 <sup>c</sup>	-40.0 ± 2.5 <sup>d</sup>	-33.5 ± 1.7 <sup>e</sup>	-20.0 <sup>f</sup>	-18.9 <sup>g</sup>	+7.0 ± 1.7 <sup>h</sup>
calcd <sup>i</sup>	-73.3	-52.3	-43.0	-33.1	-21.0	-17.9	+9.4

<sup>a</sup> Experimental  $\Delta H_f^\circ$  for isolated fragments (Ac and Et<sup>•+</sup>) is 309.1 kcal/mol.<sup>45</sup> <sup>b</sup> From  $\Delta H_f^\circ = 26.0 \pm 0.2$  kcal/mol<sup>46</sup> and  $I_v = I_a = 9.082 \pm 0.004$  eV.<sup>47</sup> <sup>c</sup> From  $\Delta H_f^\circ = 37.5 \pm 0.4$  kcal/mol<sup>48</sup> and  $I_{v,1} = 9.43 \pm 0.02$  eV.<sup>49</sup> <sup>d</sup> From  $\Delta H_f^\circ = 48.0 \pm 0.4$  kcal/mol<sup>48</sup> and  $I_{v,1} = 9.6 \pm 0.1$  eV.<sup>49</sup> <sup>e</sup> From  $\Delta H_f^\circ = 61.4 \pm 0.5$  kcal/mol<sup>8</sup> and  $I_a = 9.28 \pm 0.05$  eV.<sup>8</sup> <sup>f</sup> Assuming C<sub>4</sub>H<sub>5</sub><sup>+</sup> = methylocyclopropenium;  $\Delta H_f^\circ = 237$  kcal/mol from the appearance energy of C<sub>4</sub>H<sub>5</sub><sup>+</sup> from 1-butyne radical cation (no error limits given).<sup>50</sup> <sup>g</sup> From  $\Delta H_f^\circ(\text{cyclopropenium}) = 257$  kcal/mol (no error limits given)<sup>45</sup> and  $\Delta H_f^\circ(\text{CH}_3^\bullet) = 35.1 \pm 0.2$  kcal/mol.<sup>51</sup> <sup>h</sup> From  $\Delta H_f^\circ(\text{propargyl}) = 81 \pm 1$  kcal/mol,<sup>51</sup>  $I_{a,1}(\text{propargyl}) = 8.67 \pm 0.02$  eV,<sup>52</sup> and  $\Delta H_f^\circ(\text{CH}_3^\bullet) = 35.1 \pm 0.2$  kcal/mol.<sup>51</sup> <sup>i</sup> RCCSD(T)/cc-pVTZ single-point energies, corrected for differences of ZPE as well as integrated heat capacities to 298 K on the basis of B3LYP/6-31G\* structures and vibrational data.

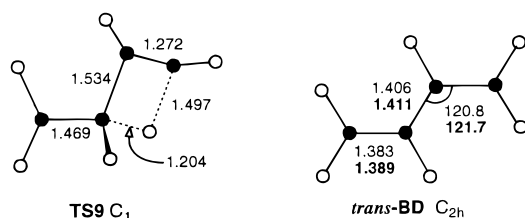


Figure 4. Structures of *trans*-BD and the transition state, TS9, connecting it to LC, which only exists on the UMP2 surface (normal, UMP2; bold, B3LYP; bond lengths in Å, angles in deg).

leads directly to *trans*-BD, thus bypassing CC. However, the barrier for this process (cf. TS9 in Figure 4) is over 10 kcal/mol, in contrast to the decay of LC to CC, which appears to be activationless (see above). Therefore, this hydrogen shift does not represent a competitive reaction, in contrast to the case of the (Et)<sub>2</sub><sup>•+</sup> linear complex where it represents the lowest energy deactivation pathway.<sup>17</sup>

The other reaction passes through an intermediate, 3-buten-3-ylum-1-yl (BU1, see Figure 5), which appears in the form of two automeric C<sub>1</sub> minima, slightly distorted from C<sub>s</sub> and interconnected by a very low-lying symmetric transition state at all levels. BU1 is reached from LC by a [1,2] hydrogen transfer in the acetylenic part, which results in a stabilization

by about 7.5 kcal/mol. This reaction involves transition state TS10, which lies 2.4 kcal/mol below TS9 for the above-described [1,3] H transfer, but it is still nearly 8 kcal/mol above LC at the RCCSD(T) level.

BU1 is a shallow minimum at UMP2 and B3LYP, but it is easily transformed to *cis*-BD by another [1,2] H shift via transition state TS11, which lies 1–2 kcal/mol above BU1 at these levels. RCCSD(T) single-point calculations even place TS11 below BU1, so it may well be that this intermediate does not exist. Since there is no a priori reason why BU1 should decay preferentially to *cis*-BD (as found by IRC calculations), we searched for another transition state leading to *trans*-BD. However, we failed to find this, so we assume that there must be a bifurcation point close to TS11 which effects distribution of the molecules into the two channels leading to *cis*- and *trans*-BD.

By accident, we found another, much more stable 3-buten-3-ylum-1-yl type structure, BU2, which arises when both pairs of hydrogens at the terminal carbons of BU1 are rotated by about 90°, whereupon the C1–C2–C3 angle diminishes by about 40° (see Figure 5). BU2 is a minimum at all levels but—unlike BU1—does not show any distortion from C<sub>s</sub> symmetry. The spin and charge distributions are surprisingly similar in the two BU species, but they differ, of course, in the orientation of

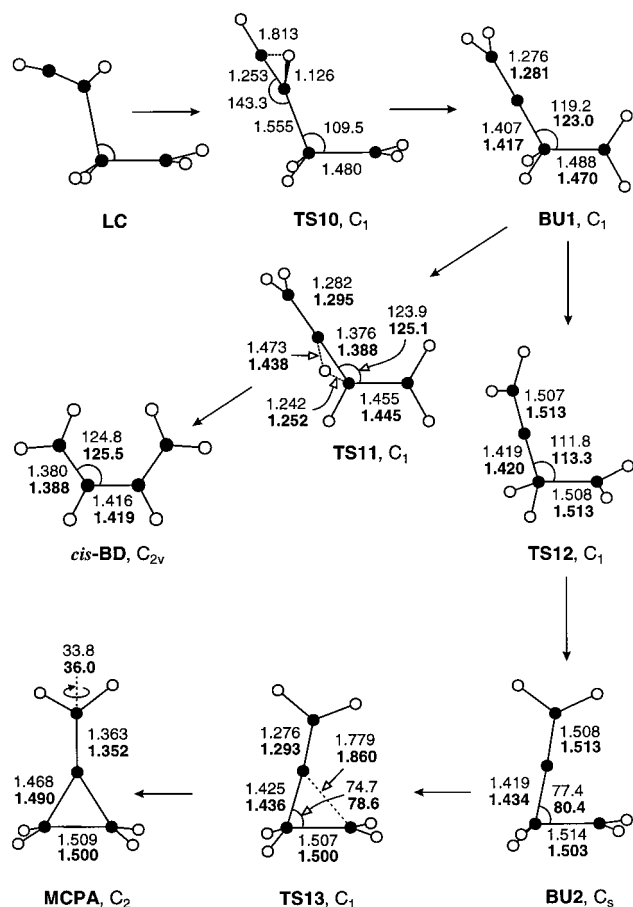


**Figure 5.** Interconnection and structures of stationary points involved in the transformation of LC to *cis*-BD or MCPA, respectively (normal, UMP2; bold, B3LYP; bond lengths in Å, angles in deg).

the p-AOs which constitute the SOMO. Despite the close kinship of the two geometric isomers, all standard methods for locating the transition state connecting them failed. After countless trials, a grid of points obtained in the space of two judiciously chosen internal coordinates led us to a saddle point (TS12, imaginary modes at  $-630$  and  $-281$   $\text{cm}^{-1}$  by B3LYP and UMP2, respectively) which looks very much like the expected elusive transition state, but all attempts to relate it to reactants or products by IRC calculations failed.

On the basis of TS12, the activation enthalpy for the transformation of BU1 to BU2 is, however, less than 1 kcal/mol at the UMP2 and RCCSD(T) levels, so BU1 appears to be another of these fleeting intermediates on the way to more stable  $\text{C}_4\text{H}_6^+$  isomers. On the other hand, BU2 is poised, both from its C–H connectivities and from the close proximity of the  $\text{CH}_2$  group to the central allenic carbon, to collapse to MCPA. Indeed, a slight shortening of this distance leads to a very low-lying transition state for this process, TS13 (imaginary modes at  $-194$  and  $-417$   $\text{cm}^{-1}$  at B3LYP and UMP2, respectively), which disappears on inclusion of zero-point energies.<sup>53</sup> MCPA itself is a stable product, but, due to the vibronic interactions which are typical of olefinic radical cations, its symmetry is reduced from  $C_2$  in the neutrals by an  $\approx 35^\circ$  torsion around the double bond.

The significance of the sequence of reactions described above and illustrated in Figure 5 is that it represents the lowest energy pathway leading to MCPA. Although nearly activationless processes were shown to lead from the weakly bound complexes to CB and *cis*-BD, the intermediate formation of MCPA cannot be completely discounted on the basis of the present results.

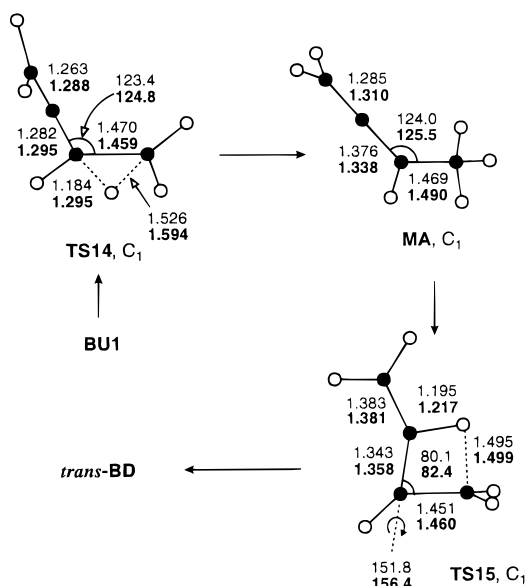


**Figure 6.** Interconnection and structures of stationary points involved in the transformation of BU1 to MA and MA to *trans*-BD (normal, UMP2; bold, B3LYP; bond lengths in Å, angles in deg).

Another stable species to which BU1 can rearrange by a simple 1,2-hydrogen shift is the 1,2-butadiene (methylallene, MA) radical cation, which might serve as a direct precursor in the ultimate fragmentation to  $\text{C}_3\text{H}_3^+ + \text{CH}_3^*$ . Indeed, a corresponding transition state, TS14 (see Figure 6, imaginary modes of  $-860$  and  $-1545$   $\text{cm}^{-1}$  at B3LYP and UMP2, respectively), was found about 5 kcal/mol above BU1. MA has no symmetry at all levels because of the rotation in the ionized allene moiety, due to the vibronic interactions which express themselves in the Jahn–Teller distortion of the parent allene radical cation. Transition state TS15 (see Figure 6, imaginary modes of  $-736$  and  $-774$   $\text{cm}^{-1}$  at B3LYP and UMP2, respectively) for the 1,3-H shift leading from MA to *trans*-BD was also located, but the barrier for this process is over 40 kcal/mol.

**3.2.3. Alternative Rearrangements of CC.** As mentioned above, CC represents a metastable intermediate on the way from  $\text{Et}^+ + \text{Ac}$  to CB. As in the other cases, we also explored the reaction channels corresponding to hydrogen shifts in CC. The first one is for a transfer of a H atom in the three-membered ring from the CH group to a  $\text{CH}_2$  group. This is accompanied by ring opening to eventually form BTY.<sup>54</sup> The concerted nature of the H shift and ring opening becomes evident from transition state TS16 (see Figure 7, imaginary modes of  $-394$  and  $-661$   $\text{cm}^{-1}$  at B3LYP and UMP2, respectively), which shows that the formation of the new C–H bond occurs simultaneously to the weakening of the C–C bond that is eventually broken. However, the activation barrier for that process is almost 30 kcal/mol, so it is unlikely to be competitive with the other rearrangements described above. Hence, the formation of BTY, i.e., a possible precursor to the propargyl cation, in the  $\text{Et}^+ + \text{Ac}$  reaction is very improbable.

The same hydrogen atom can be shifted to the exocyclic, formally divalent carbon to yield MCPA. The transition state for this reaction (TS17, imaginary modes of  $-394$  and  $-661$   $\text{cm}^{-1}$  at B3LYP and UMP2, respectively) is very early on the reaction coordinate, and the only change in the C–C bonds is the shortening of the exocyclic one, which gives the double bond in the product. But once again, the activation barrier for this process (27 kcal/mol at the RCCSD(T) level) is much too

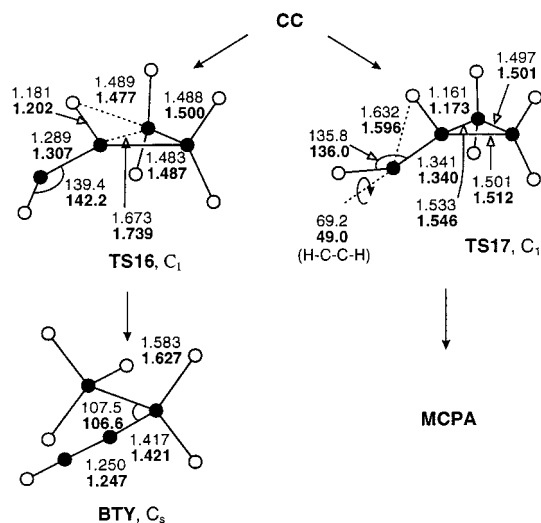


**Figure 7.** Interconnection and structures of stationary points involved in the transformation of CC to MCPA and to BTY, respectively (normal, UMP2; bold, B3LYP; bond lengths in Å, angles in deg).

high to allow this process to compete with the formation of MCPE via BU1 (see above).

**3.2.4. Rearrangements of *cis*-BD to MCPE.** Unless the observed ultimate fragmentation to C<sub>3</sub>H<sub>3</sub><sup>+</sup> + CH<sub>3</sub><sup>•</sup> involves a concerted loss of CH<sub>2</sub> and H (which appears unlikely), it requires a preceding rearrangement of the incipient radical cations (CH<sub>2</sub>)<sub>2</sub>(CH)<sub>2</sub> to those with a (CH)<sub>3</sub>(CH<sub>3</sub>) pattern of connectivities. Therefore, we wanted to find the transition states for all possible H shifts for such rearrangements. We have already described above two such processes (the one leading from BU1 via TS14 to MA and that leading from CC via TS16 to BTY), but both are associated with rather high activation barriers and are unlikely to be competitive with the nearly activationless decays to CB or BD.

The most obvious such rearrangement involves a 1,4-hydrogen shift in *cis*-BD to give a propenylcarbene radical cation (PRC) that would subsequently collapse to yield MCPE, certainly a very attractive direct precursor of C<sub>3</sub>H<sub>3</sub><sup>+</sup> + CH<sub>3</sub><sup>•</sup>. This pathway has been recognized and explored at the UMP2 level by Keister et al.<sup>8</sup> We confirmed their findings and went on to apply our standard methodology to this process. The results, shown in Figure 8 and Table 2, indicate that it is associated with a barrier of almost 50 kcal/mol. About 60% of this is due to the endothermicity of the BD → PRC rearrangement, and the 17 kcal/mol barrier for the reverse process is mostly due to the fact that the H transfer occurs over such a large distance that a good part of the CH bond dissociation energy must be invested before any bonding interaction to the formally divalent accepting C atom begins to develop.

Transition state TS18 (imaginary modes of  $-1396$  and  $-1811$  cm<sup>-1</sup> at B3LYP and UMP2, respectively) for this rearrangement shows the expected features of being close to the product, MVC, and strongly reduced C–C–C angles to maximize the bonding interactions to the migrating hydrogen atom. As expected (and found by Keister et al.), PRC is poised for collapse to MCPE, but due to the strong ring strain which prevails in the latter compound, this process is endothermic by about 8 kcal/mol. Transition state TS19 (Figure 8, imaginary modes of  $-170$  and  $-379$  cm<sup>-1</sup> at B3LYP and UMP2, respectively) lies very close to MCPE and only 0.05 kcal/mol above it by RCCSD(T)//UMP2.

Our RCCSD(T)/cc-pVTZ prediction for  $\Delta_f H^\circ$  of MCPE (from the data in Table 3) is 276 kcal/mol, in excellent accord with

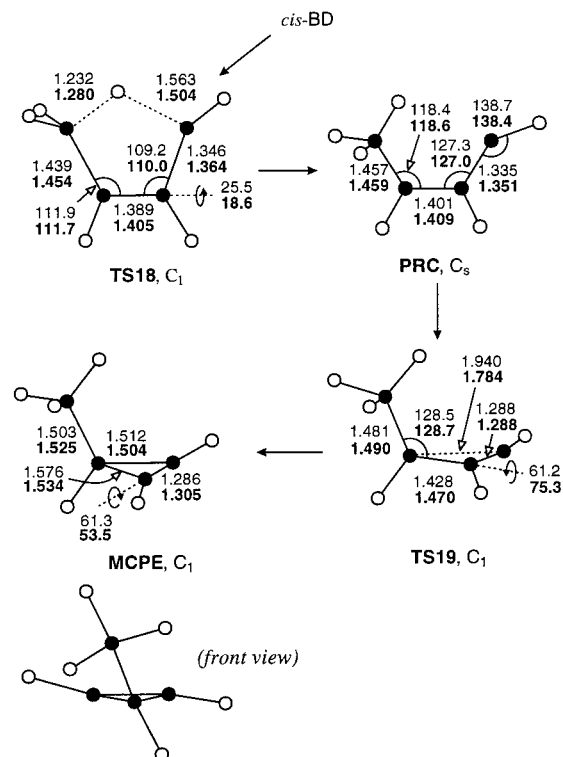


**Figure 8.** Interconnection and structures of stationary points involved in the transformation of *cis*-BD to MCPE (normal, UMP2; bold, B3LYP; bond lengths in Å, angles in deg). Bottom: alternate view of MCPE.

the experimental value of  $275.6 \pm 1.2$  kcal/mol given by Keister et al.<sup>8</sup> To compare our result with those obtained by UMP2 with a similar basis set,<sup>8</sup> we should consider  $\Delta E_0$  for the *trans*-BD → MCPE reaction, for which we obtain  $\Delta E_0 = 40.0$  kcal/mol (experimental  $\Delta H_{298} = 40.5 \pm 1.7$  kcal/mol), as compared to 35.4 kcal/mol by UMP2. Interestingly, the RMP2/6-31G\* prediction for the same reaction is nearly identical with that obtained at our reference level of theory. Although this agreement is perhaps a bit fortuitous, it clearly demonstrates the problems of UMP2 with rearrangements involving open-shell species where the UHF wave function shows different degrees of spin contamination:  $\langle S^2 \rangle$  is nearly 1 in *trans*-BD but only 0.78 in MCPE, which clearly puts the former species at an energetic disadvantage relative to the latter, thus resulting in a too small isomerization energy. On the other hand, B3LYP overestimates  $\Delta E_0$  for this process by about 4 kcal/mol.

We were surprised to find that the equilibrium structure of MCPE is strongly distorted from the (average) C<sub>s</sub> symmetry, which prevails in the neutral (see separate view at the bottom of Figure 8). As it turns out, the C<sub>s</sub> structure is a transition state for interconversion of two C<sub>1</sub> minima (over a barrier of 3.5 kcal/mol by UMP2). The reason for this distortion can be traced back to a vibronic interaction between an A' state and an A'' state, where the unpaired electron occupies the singly occupied  $\pi$ -MO (HOMO) or the subjacent antisymmetric  $\sigma_{C-C}$  MO (HOMO-1), respectively (see Figure 9). Distortion from C<sub>s</sub> symmetry allows these two states to mix. This expresses itself very clearly in the HOMO at the equilibrium geometry of MCPE, which really looks like a linear combination of the two highest occupied MOs in C<sub>s</sub>. As we have shown in the example of the CB ring opening, such vibronic interactions are quite common in radical cations with their low-lying excited states, and they may have a profound influence on the shapes of the potential energy surfaces.<sup>33</sup>

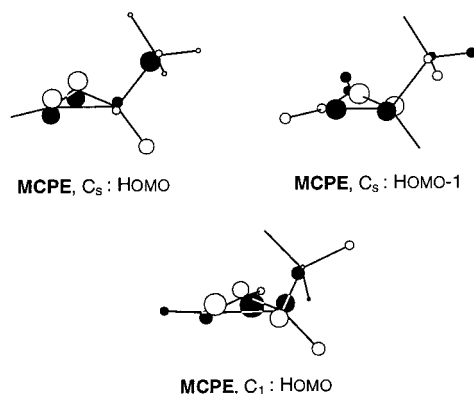


**Figure 9.** HOMO and HOMO-1 of MCPE in  $C_{3v}$  symmetry and HOMO of the same compound at its nonsymmetric equilibrium geometry (cf. Figure 8).

**3.3. Fragmentation Channels.** **3.3.1. Cyclopropenium Cation (CPR) +  $CH_3^*$ .** Apart from the ring opening of CB, the  $C_4H_6^{*+}$  PES received the most attention in the literature in connection with the methyl loss reactions of  $C_4H_6^{*+}$  ions. There is every reason to believe that the precursor for this fragmentation is a  $C_4H_6^{*+}$  structure carrying a methyl group, because it is hardly conceivable that a concerted reaction involving C–C bond breaking accompanied by a hydrogen atom transfer would be kinetically competitive with simple C– $CH_3$  bond cleavage.

Since CPR is the more stable of the two possible  $C_3H_3^+$  structures, MCPE appears to be the most plausible precursor for the methyl loss reaction. Indeed, it was concluded many years ago from scattering diagrams for the process  $Ac^{*+} + Et \rightarrow [C_4H_6^{*+}] \rightarrow C_3H_3^+ + CH_3^*$  that the last intermediate on the pathway to the ultimate fragments should have a structure close to MCPE.<sup>2,3</sup> This is in accordance with the experimental evidence (summarized in ref 8) that  $C_4H_6^{*+}$  ions of different structures lose  $CH_3^*$  by prior isomerization to a higher energy structure, which is usually assumed to be MCPE. Before the completion of the present paper, Keister et al.<sup>8</sup> supported this hypothesis by UMP2/6-311G\*\* calculations. Although we basically arrived at similar conclusions, we would like to present our results because our calculations were carried out on a higher level and we can provide some interesting additional details.

As noted already by Keister et al.,<sup>8</sup> elongation of the C–C bond in the course of dissociation of MCPE is not associated with a monotonic increase in energy. On the way to the fragments, they encountered a  $[CPR \cdots CH_3^*]$  ion–molecule complex whose structure they did, however, not specify. We found this to correspond to the species C1 in Figure 10, where the unpaired electron resides in the bonding combination between one component of the degenerate cyclopropenium  $\pi$ -MO and the  $CH_3^*$  SOMO. It has a methyl–ring C–C distance of  $d = 2.9 \text{ \AA}$ , while the angle  $\alpha$  between the plane of the CPR ring and the methyl carbon is  $111^\circ$ . It is a minimum at all levels except B3LYP, where it does not exist as a stationary point. Transition state TS20, which connects MCPE to C1, lies less than 1 kcal/mol above C1 (slightly more if the ZPE correction is based on UMP2 frequencies), so this complex is barely protected from collapse to MCPE.

In addition to C1, we found another  $[CPR \cdots CH_3^*]$  complex in which the methyl radical is positioned *in the plane of CPR* ( $d = 3.4 \text{ \AA}$ ,  $\alpha = 180^\circ$ ). The bonding in this complex, which is about 1 kcal/mol more stable than C1, is entirely different from that which prevails in C1 and corresponds to a hydrogen bridge between CPR and the p-AO of the methyl radical, similar to that found in the acetylene dimer cation.<sup>33</sup> C2 exists as a

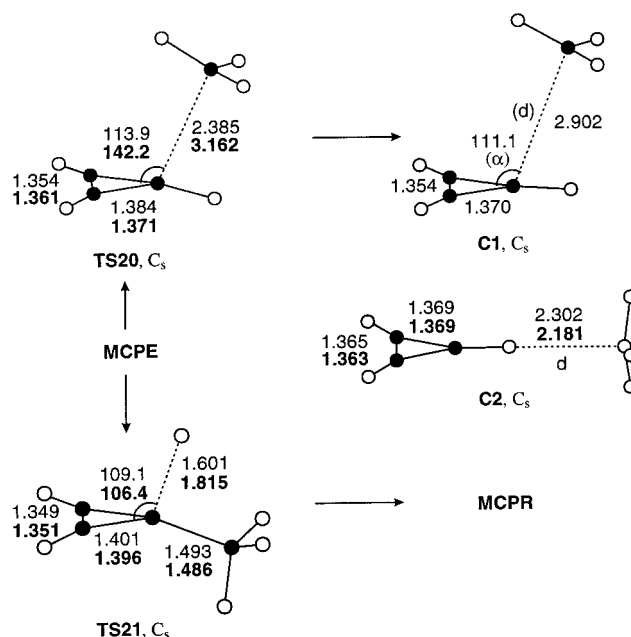


**Figure 10.** Structures of  $[C_3H_3^+ \cdots CH_3^*]$  ion–molecule complexes C1 and C2 and the transition state, TS20, connecting them to MCPE (normal, UMP2; bold, B3LYP; bond lengths in  $\text{\AA}$ , angles in deg).

minimum at all levels including B3LYP, where we also found a transition state (imaginary mode at  $-94 \text{ cm}^{-1}$ ) which connects it to MCPE. All attempts to locate this transition state at other levels failed, so we conclude that C2 is connected to MCPE via C1. However, we did not consider it expedient to locate the transition state connecting the two complexes, a task which would have been quite arduous in view of the flatness of the potential energy surface and did not promise to provide much additional insight.

Starting from C1 or C2, the energy rises smoothly to the dissociation products, CPR +  $CH_3^*$ . Compared to the UMP2 calculations of Keister et al.,<sup>8</sup> we also achieved a considerable improvement in the prediction of the threshold for methyl loss from BD. Relative to *trans*-BD,  $\Delta E_0$  of the dissociation products is now 53.9 kcal/mol (experimental  $\Delta H_{298} = 55.3 \pm 0.3 \text{ kcal/mol}$ <sup>8</sup>), compared to 48 kcal/mol by UMP2, which testifies once more to the problems of UMP2 with spin-contaminated species. If we take  $\Delta E_0$  relative to the starting  $Et^{*+} + Ac$ , then the discrepancy between the RCCSD(T) and the UMP2 results is much less pronounced (cf. Table 4).

**3.3.2. Propargyl Cation (PRG) +  $CH_3^*$ .** Although CPR is over 25 kcal/mol more stable than its open-chain isomer, propargyl cation, PRG, the latter (combined with  $CH_3^*$ ) still lies below  $Ac^{*+} + Et$ , the compounds used in the crossed-beam experiments of Herman et al.<sup>2,3</sup> (note from Table 4 that PRG +  $CH_3^*$  lie *above*  $Et^{*+} + Ac$ , but Table 1 gives an energy of +20 kcal/mol for the charge-exchange process). Two  $C_4H_6^{*+}$  isomers must be taken into account as precursors for this fragmentation, BTY and MA. However, the transition states for methyl loss from both ions have a quasilinear structure which is incompatible with the experimental findings, so we did not pursue these channels in any more detail. However, we note that the energy difference between the two  $C_3H_3^+$  isomers (experimental  $\Delta H_{298} = 25.9 \pm 2 \text{ kcal/mol}$ ) is rather well reproduced by RCCSD(T) ( $\Delta E_0 = 26.8 \text{ kcal/mol}$ ), whereas MP2 ( $\Delta E_0 = 31.4 \text{ kcal/mol}$ ) is once more off the mark, in contrast to B3LYP ( $\Delta E_0 = 25.3 \text{ kcal/mol}$ ).

**3.3.3.  $C_4H_5^+ + H^*$ .** The second fragmentation channel observed in the crossed-beam experiments of Herman et al.<sup>2,3</sup>

**TABLE 4: Energies and 0 K Enthalpies (kcal/mol) Relative to Ac + Et<sup>•+</sup> of Structures Involved in the Fragmentation of C<sub>4</sub>H<sub>6</sub><sup>•+</sup>**

structure <sup>a</sup>	B3LYP/6-31G*		(R)MP2/6-31G*		UMP2/6-31G*		(R)CCSD(T)/cc-pVTZ	
	$\Delta E$	$\Delta E_0$	$\Delta E$	$\Delta E_0^b$	$\Delta E$	$\Delta E_0$	$\Delta E$	$\Delta E_0^c$
MCPE	-41.16	-38.22	-40.12	-35.89	-37.64	-33.42	-34.83	-31.89
TS20: MCPE → C1	-25.15 <sup>d</sup>	-24.40 <sup>d</sup>	-25.53	-22.84	-25.28	-22.58	-21.75	-21.00
C1	<sup>e</sup>	<sup>e</sup>	-26.00	-24.14	-26.01	-24.15	-22.32	-20.46
C2 (H-bonded)	-25.76	-24.82	-26.92	-25.09	-26.97	-25.15	-22.55	-21.61
CPR + CH <sub>3</sub> <sup>•</sup>	-19.41	-19.81	-21.20	-20.96	-21.31	-21.06	-17.58	-17.97
PRG + CH <sub>3</sub> <sup>•</sup>	7.30	5.46	11.65	10.49	11.54	10.38	10.70	8.86
TS21: MCPE → MCPR	-18.35	-18.37	-21.86	-20.73	-21.30	-20.17	-13.18	-13.19
MCPR + H <sup>•f</sup>	-36.78	-38.19	-23.35	-24.76			-19.57	-20.98
CBY + H <sup>•f</sup>	-16.10	-16.31	-12.35	-12.56			-10.98	-10.58
MEA + H <sup>•f</sup>	-3.70	-5.98	-10.41	-12.70			-4.08	-6.36

<sup>a</sup> For UMP2 and B3LYP optimized structures, see Figures 8–11; structures TS<sub>x</sub> are transition states. <sup>b</sup> ZPE differences from UMP2 vibrations. <sup>c</sup> ZPE differences from B3LYP. <sup>d</sup> TS between MCPE and C2, discussion see text. <sup>e</sup> Not found at B3LYP. <sup>f</sup> With  $E(\text{H}^\bullet) = 0.5$  hartrees, (hence no entry for UMP2).

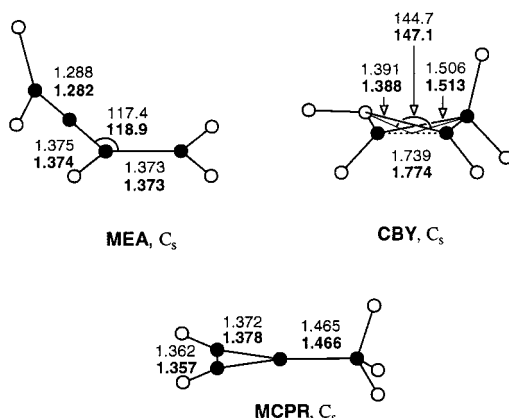


**Figure 11.** Structures of the three most stable C<sub>4</sub>H<sub>5</sub><sup>+</sup> isomers, MEA, CBY, and MCPR (normal, UMP2; bold, B3LYP; bond lengths in Å, angles in deg).

corresponded to loss of atomic hydrogen. Exploratory B3LYP calculations indicated that only three C<sub>4</sub>H<sub>5</sub><sup>+</sup> isomers are energetically accessible from Ac<sup>•+</sup> + Et. They correspond to loss of H<sup>•</sup> from MCPE, CB, or MA, which yields methylcyclopropenium cation (MCPR), cyclobutenium cation (CBY), or methyleneallene cation (MEA), respectively (see Table 4 and Figure 11). The last of these structures can be excluded on the basis of the observed scattering diagrams which can, however, not distinguish between the former two possibilities.

Our calculated energy of the most stable of these fragments, MCPR + H<sup>•</sup> relative to Et<sup>•+</sup> + Ac, is in excellent accord with experiment (cf. Table 3). However, in contrast to the methyl loss channels, no ion–molecule complex is involved in hydrogen loss, which leads to the replacement of the corresponding minimum by a transition state (TS21) which lies about 8 kcal/mol above the fragments, thus implying a corresponding activation barrier for the reverse process. In view of the nearly activationless addition of CH<sub>3</sub><sup>•</sup> to CPR and the fact that the exothermicities of both processes are quite similar (14 vs 11 kcal/mol), this result is rather surprising. We found that addition of H<sup>•</sup> to CPR, or to the unsubstituted carbon of MCPR, is also nearly activationless;<sup>55</sup> therefore, the activation barrier encountered by H<sup>•</sup> in the attack at the methyl-substitution site may be traced to the disruption of the hyperconjugative stabilization of CPR by the methyl group.

Another way to view this phenomenon is by reference to the MOs depicted in Figure 9: TS20 and TS21 connect adiabatically to the ground state of MCPE, where the SOMO is much more strongly bonding along the CPR–CH<sub>3</sub> bond. This expresses itself also in the elongated exocyclic C(sp<sup>2</sup>)-C(sp<sup>3</sup>) bond in

MCPE. Thus, the transition state for loss of CH<sub>3</sub><sup>•</sup> is closer to the reactant than that for loss of H<sup>•</sup>, and hence, the activation barrier for the former process is smaller.

In view of the fact that TS21 for H<sup>•</sup> loss from MCPE lies below the energy of the other possible C<sub>4</sub>H<sub>5</sub><sup>+</sup> isomer, CBY (+ H<sup>•</sup>) indicates that the formation of MCPR represents the lowest energy channel for H<sup>•</sup> loss. Therefore, we did not pursue the higher lying pathway leading to CBY + H<sup>•</sup>.

#### 4. Conclusions

This is the last of a series of three papers on the formation, rearrangement, and subsequent redissociation of ion–molecule complexes involving ethylene and acetylene.<sup>17,33</sup> The three cases we have treated show some similarities, but also some surprising differences, which demonstrates that general rules governing the reactivity of radical cations are not as easy to obtain as in the case of neutral closed-shell molecules. Rather close analogies can be seen between the behavior of (Ac)<sub>2</sub><sup>•+</sup> and the present (Et<sup>•</sup>Ac)<sup>•+</sup> complexes. In both cases, we see a nearly activationless collapse of the incipient ion–molecule complex to stable four-membered-ring structures. Although these arise formally by a 2π + 2π cycloaddition of the reactants, the actual course of the reaction is, in both cases, a highly nonconcerted one, leading to several highly metastable intermediates. The last of these is a species which may be regarded as a cycloprop(en)yl carbene cation (CC).

In the present case, several alternative pathways for the rearrangement of some of these intermediates were explored, but they invariably involve rather high-lying transition states and thus do not appear to compete with the rearrangements starting from the primary stable product, i.e., the cyclobutene radical cation (CB). The ring opening of CB to butadiene radical cation (BD) occurs quite readily ( $E_a \approx 18$  kcal/mol<sup>7</sup>), but any formation of other stable C<sub>4</sub>H<sub>6</sub><sup>•+</sup> isomers with different C–H connectivities involves much higher activation barriers. Three such processes were found to lead from *cis*-BD to tautomers poised for fragmentation to C<sub>3</sub>H<sub>3</sub><sup>+</sup> + CH<sub>3</sub><sup>•</sup>, i.e., the fragments observed in the crossed-beam studies of Herman et al.<sup>2,3</sup> (see Figure 12).

Two of these processes involve similar barriers of about 45 kcal/mol. The first is a direct 1,4-hydrogen transfer to give an intermediate best regarded as a propenylcarbene cation (PRC). The second follows a sequence of two 1,2-H transfers, the first one to give a distonic radical cation CH<sub>2</sub>–C<sup>+</sup>–CH<sub>2</sub>–CH<sub>2</sub><sup>•</sup>, BU1, followed by another one yielding methylallene, MA. Instead of undergoing the second of these H transfers, the intermediate BU1 can cyclize via a very low-lying transition state to the

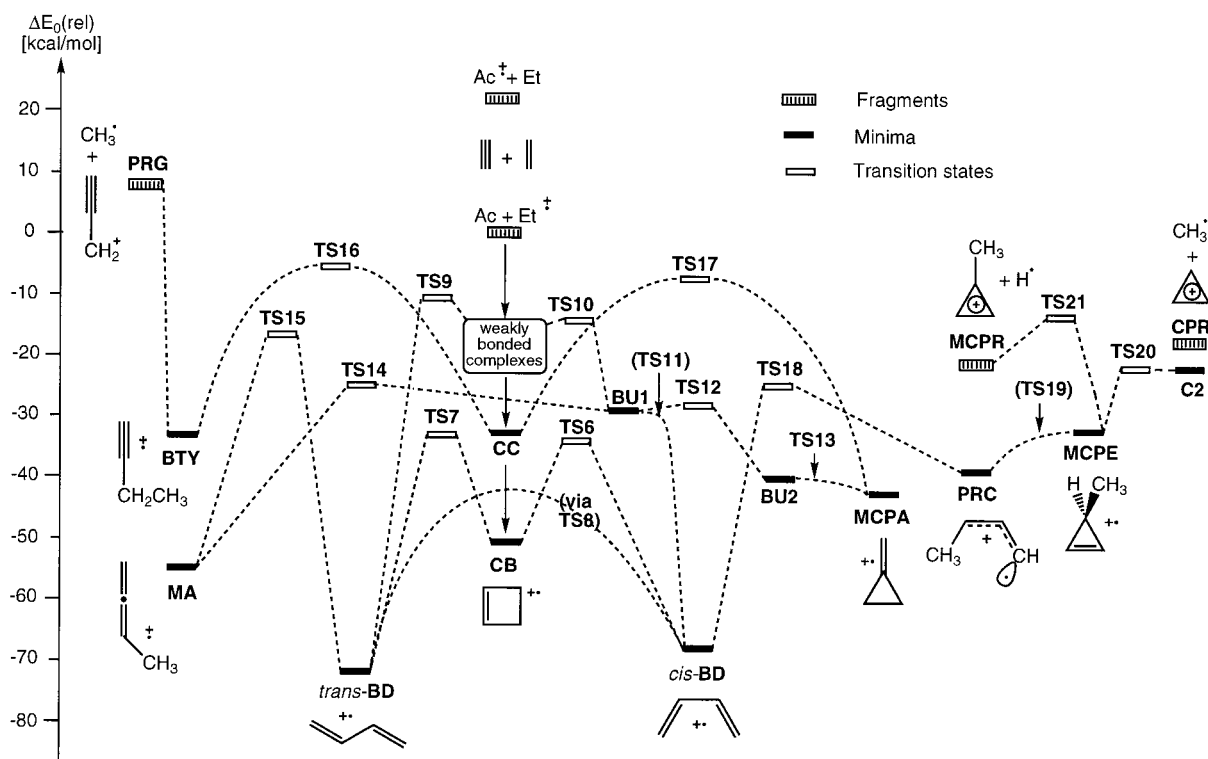


**Figure 12.** Schematic representation of the potential energy surface on which the  $\text{Et}^+ + \text{Ac}$  reaction and the subsequent rearrangements and fragmentations discussed in this study take place. Energies relative to  $\text{Et}^+ + \text{Ac}$  are from single-point RCCSD(T)/cc-pVTZ calculations at B3LYP/6-31G\* geometries, corrected for ZPE differences on the basis of frequencies calculated at the same level (cf. Tables 1–4). Transition states which lie at lower energies than reactants at this level are indicated by vertical arrows. For details of the region labeled “weakly bonded complexes”, cf. Schemes 1 and 2 and Table 1.

methylenecyclopropane radical cation, MCPA, which can, however, not lose  $\text{CH}_3$  in a simple fragmentation process.

Formation of the third  $\text{C}_4\text{H}_6^+$  isomer carrying a methyl group, 1-butyne radical cation, BTY, requires much higher activation and was not considered in detail. Instead, we concentrated on the methyl loss reaction from PRC which occurs after intermediate cyclization to the methylcyclopropene radical cation, MCPE, to yield the most stable  $\text{C}_3\text{H}_3^+$  isomer, the cyclopropenium cation, CPR. This mechanism is in accord with experimental observations,<sup>2,3,8</sup> and it involves formation of a  $[\text{CPR} \cdots \text{CH}_3^+]$  ion–molecule complex which comes in two forms, C1 and C2, of entirely different nature but very similar energy. The fragmentation of MA leads to the much less stable propargyl cation (PRG), and its mechanism was not considered in detail because it is incompatible with the observed scattering diagrams.<sup>2,3</sup>

Finally, we considered different cleavages leading to  $\text{C}_4\text{H}_5^+ + \text{H}^+$ , the other pair of fragments observed in the crossed-beam studies.<sup>2,3</sup> The most stable  $\text{C}_4\text{H}_5^+$  isomer is the methylcyclopropenium cation (MCPR), which may be formed readily from MCPE in a process which does, however, not involve an ion–molecule complex of any sort. Two other  $\text{C}_4\text{H}_5^+$  species, the cyclobutenium cation, CBY, and the methyleneallene cation, MEA, lie 10–12 kcal/mol higher in energy. They require as precursors CB or MA, respectively, both of which are accessible from  $\text{Et}^+ + \text{Ac}$  below the dissociation threshold. A reaction path via MEA may again be excluded, because it is not compatible with scattering diagrams.

**Acknowledgment.** This work has been funded through Grant No. 2028-047212.96/1 of the Swiss National Science Foundation and a grant from the Swiss Federal Office for Science and Education in the framework of COST action D3 (Theory and

Modeling of Chemical Systems and Processes) of which this joint project between the University of Fribourg (Institute of Physical Chemistry) and the Academy of Sciences of the Czech Republic (J. Heyrovský Institute) forms a part. Funding in Prague was provided by the Ministry of Education of the Czech Republic. We thank the Swiss Center for Scientific Computing in Manno for a generous allocation of CPU time on the NEC SX-3/SX4 supercomputer, without which the coupled cluster calculations would have been impossible to carry out.

**Supporting Information Available:** Tables containing the UMP2 and B3LYP total energies, thermal corrections, and Cartesian coordinates of all stationary points (minima and transition states) discussed in this study, in ASCII format, are available through the Internet. See any current masthead page for Web access instructions.

## References and Notes

- (1) Baer, T. In *Gas-Phase Ion Chemistry*; Bowers, M. T., Ed.; Academic: New York, 1979; Vol. 1, p 153.
- (2) Herman, Z. Unpublished results.
- (3) Herman, Z.; Birkinshaw, K. *Ber. Bunsen-Ges. Phys. Chem.* **1973**, *77*, 566.
- (4) Du, P.; Borden, W. T. *J. Am. Chem. Soc.* **1987**, *109*, 5330.
- (5) Belville, D. J.; Chelsky, R.; Bauld, N. L. *J. Comput. Chem.* **1982**, *3*, 548.
- (6) Wiest, O. *J. Am. Chem. Soc.* **1997**, *119*, 5713.
- (7) Sastry, G. N.; Bally, T.; Hrouda, V.; Carsky, P. *J. Am. Chem. Soc.* **1998**, *120*, 9323.
- (8) Keister, J. W.; Baer, T.; Evans, M.; Ng, C. Y.; Hsu, C. W. *J. Phys. Chem. A* **1997**, *101*, 1866.
- (9) Werner, A. S.; Baer, T. *J. Chem. Phys.* **1978**, *62*, 2900.
- (10) Bunn, T. L.; Baer, T. *J. Chem. Phys.* **1986**, *85*, 6361.
- (11) Preuninger, F. N.; Farrar, J. M. *J. Chem. Phys.* **1982**, *77*, 263.
- (12) Dannacher, J.; Flamme, J. P.; Stadelmann, J.-P.; Vogt, J. *J. Chem. Phys.* **1980**, *51*, 189.

- (13) Bombach, R.; Dannacher, J.; Stadelmann, J.-P. *J. Am. Chem. Soc.* **1983**, *105*, 1824.
- (14) Sellers-Hann, L.; Kreiller, R. E.; Russell, D. H. *J. Chem. Phys.* **1988**, *89*, 889.
- (15) Russell, D. H.; Gross, M. L.; Greef, J. V. d.; Nibbering, N. N. M. *J. Am. Chem. Soc.* **1979**, *101*, 2086.
- (16) Bally, T.; Borden, W. T. In *Reviews in Computational Chemistry*; Lipkowitz, K. B., Boyd, D. B., Eds.; VCH: New York, 1999; Vol. 13 (in print).
- (17) Jungwirth, P.; Bally, T. *J. Am. Chem. Soc.* **1993**, *115*, 5783.
- (18) Frisch, M. J.; Trucks, G. W.; Schlegel, H. B.; Gill, P. M. W.; Johnson, B. G.; Robb, M. A.; Cheeseman, J. R.; Keith, T.; Petersson, G. A.; Montgomery, J. A.; Raghavachari, K.; Al-Laham, M. A.; Zakrzewski, V. G.; Ortiz, J. V.; Foresman, J. B.; Cioslowski, J.; Stefanov, B. B.; Nanayakkara, A.; Challacombe, M.; Peng, C. Y.; Ayala, P. Y.; Chen, W.; Wong, M. W.; Andres, J. L.; Repogle, E. S.; Gomperts, R.; Martin, R. L.; Fox, D. J.; Binkley, J. S.; DeFrees, D. J.; Baker, J.; Stewart, J. P.; Head-Gordon, M.; Gonzales, M. C.; Pople, J. A.; Gaussian 94, Version B1 and D4; Gaussian, Inc.: Pittsburgh, PA, 1995.
- (19) Schmidt, M. W.; Baldrige, K. K.; Boatz, J. A.; Elbert, S. T.; Gordon, M. S.; Jensen, J. H.; Kosecki, S.; Matsunaga, N.; Nguyen, K. A.; Su, S. J.; Windus, T. L.; Dupuis, M.; Montgomery, J. A. *J. Comput. Chem.* **1993**, *14*, 1347.
- (20) Lee, T. J.; Rendell, A. P.; Dyal, K. G.; Jayatilaka, D. *J. Chem. Phys.* **1994**, *100*, 7400.
- (21) Lauderdale, W. J.; Stanton, J. F.; Gauss, J.; Watts, J. D.; Bartlett, R. J. *J. Chem. Phys. Lett.* **1991**, *187*, 21.
- (22) Amos, R. D.; Andrews, J. S.; Handy, N. C.; Knowles, P. J. *J. Chem. Phys. Lett.* **1991**, *186*, 130.
- (23) Amos, R. D.; Alberts, I. L.; Andrews, J. S.; Colwell, S. M.; Handy, N. C.; Jayatilaka, D.; Knowles, P. J.; Kobayashi, R.; Laidig, K. E.; Laming, G.; Lee, A. M.; Maslen, P. E.; Murray, C. W.; Rice, J. E.; Simandiras, E. D.; Stone, A. J.; Su, M. D.; Tozer, D. J. *Cadpac 5*; Cambridge University: Cambridge, MA, 1995.
- (24) Stanton, J. F.; Gauss, J.; Watts, J. D.; Lauderdale, W. J.; Bartlett, R. J. *Int. J. Quantum Chem. Symp.* **1992**, *26*, 879.
- (25) Hariharan, P. C.; Pople, J. A. *J. Chem. Phys. Lett.* **1972**, *16*, 217.
- (26) Knowles, P. J.; Hampel, C.; Werner, H.-J. *J. Chem. Phys.* **1993**, *99*, 5219.
- (27) Werner, H.-J.; Knowles, P. J.; Almlöf, J.; Amos, R. D.; Deegan, M. J. O.; Elbert, S. T.; Hampel, C.; Meyer, W.; Peterson, K.; Pitzer, R.; Stone, A. J.; Taylor, P. R.; Lindh, R. *MOLPRO 96.1*, 1996.
- (28) Dunning, T. H. *J. Chem. Phys.* **1989**, *90*, 1007.
- (29) Gonzales, C.; Schlegel, H. B. *J. Chem. Phys.* **1989**, *90*, 2154.
- (30) Boys, S. F.; Bernardi, F. *Mol. Phys.* **1970**, *19*, 553.
- (31) Xantheas, S. S. *J. Chem. Phys.* **1996**, *104*, 8821.
- (32) *NIST Standard Reference Database*, 69, Aug 1997 Release.
- (33) Hrouda, V.; Roeselova, M.; Bally, T. *J. Phys. Chem. A* **1997**, *101*, 3925.
- (34) This transition state exhibits one imaginary mode interconnecting two automeric PpC structures at the UMP2 level ( $-79\text{ cm}^{-1}$ ). At ROHF ( $-128$ ,  $-65\text{ cm}^{-1}$ ), UHF ( $-140$ ,  $-67\text{ cm}^{-1}$ ), and B3LYP ( $-119$ ,  $-58\text{ cm}^{-1}$ ), a second, very soft imaginary mode appears.
- (35) TS2 is a true transition state with one imaginary mode at the SCF level (frequencies of  $-606\text{ cm}^{-1}$  at ROHF,  $-150\text{ cm}^{-1}$  at UHF), leading formally to PC (which is a transition state at these levels) but connecting in practice CC with TC.
- (36) This structure which may be viewed as a distonic radical cation is called but-3-en-4-ylum-1-yl according to the standard chemical nomenclature.
- (37) UHF/6-31G\*, ROHF/6-31G\*, and UMP2/6-31G\* predict clearly that the twist structure LC is a minimum. In contrast, RMP2/6-31G\* gives an imaginary vibrational frequency, which varies greatly with a selected step size in the numerical two-sided differentiation of the RMP2 gradient ( $-1227\text{ cm}^{-1}$  for 0.001 au,  $-619\text{ cm}^{-1}$  for 0.005 au,  $-427\text{ cm}^{-1}$  for 0.01 au,  $-578\text{ cm}^{-1}$  for 0.02 au, and  $-443\text{ cm}^{-1}$  for 0.05 au). Also, the respective normal coordinate varies greatly with differing step sizes. We tried to move downhill along the normal coordinate given by the force constant matrix obtained with a step size of 0.01 au. However, no matter how small we chose the distortion, the energy was invariably higher than that of the stationary point. Therefore, we cannot decide whether LC is a minimum or not on the RMP2 surface.
- (38) By ROHF, we managed to find only TS4 ( $-297\text{ cm}^{-1}$ ) but failed to locate TS3 because of the convergence problems, whereas at UHF, we located only TS3 ( $-512\text{ cm}^{-1}$ ).
- (39) The trans conformation (dihedral angle =  $180^\circ$ ) is a transition state for the interconversion of two twisted ones, at the UMP2 level about 4.2 kcal/mol higher than the latter. Surprisingly, the SCF methods also predict the cis structure (dihedral angle =  $0^\circ$ ) to be a minimum, but this feature is not reproduced at the correlated levels and must hence be regarded as an artifact.
- (40) Ruscic, B.; Berkowitz, J.; Curtiss, L. A. *J. Chem. Phys.* **1989**, *91*, 114.
- (41) Blush, J. A.; Chen, P. *J. Phys. Chem.* **1992**, *96*, 4138.
- (42) Houle, F. A.; Beauchamp, J. A. *J. Am. Chem. Soc.* **1979**, *101*, 4067.
- (43) Bally, T.; Sastry, G. N. *J. Phys. Chem. A* **1997**, *101*, 7923.
- (44) Note that CC comes in two conformers that differ in the dihedral angle to the hydrogen atom at the divalent carbon. At all levels, the trans form is more stable than the cis form by about 1 kcal/mol. An estimate of barrier for interconversion of the two forms (about 3 kcal/mol) may be taken from on the B3LYP value calculated for CC in C<sub>4</sub>H<sub>4</sub><sup>•+</sup>.
- (45) Lias, S. G.; Bartmess, J. E.; Liebman, J. F.; Holmes, J. L.; Levin, R. D.; Mallard, W. G. *J. Phys. Chem. Ref. Data Suppl. 1* **1988**, *17*, 1.
- (46) Prosen, E. J.; Maron, F. W.; Rossini, R. D. *J. Res. NBS* **1951**, *46*, 106.
- (47) Mallard, W. G.; Miller, J. H.; Smyth, K. C. *J. Chem. Phys.* **1983**, *79*, 5900.
- (48) Wiberg, K. B.; Fenoglio, R. A. *J. Am. Chem. Soc.* **1968**, *90*, 3395.
- (49) Bieri, G.; Burger, F.; Heilbronner, E.; Maier, J. P. *Helv. Chim. Acta* **1977**, *60*, 2213.
- (50) Lossing, F. P.; Holmes, J. L. *J. Am. Chem. Soc.* **1984**, *106*, 6917.
- (51) Tsang, W. In *Energetics of Organic Free Radicals*; Simoes, J. A. M., Greenberg, A., Liebman, J. F., Eds.; Blackie Academic & Professional: London, 1996; p 22.
- (52) Minsek, D. W.; Chen, P. *J. Phys. Chem.* **1990**, *94*, 8399.
- (53) At UMP2, TS12 leads to another minimum which is separated by a second transition state from MCPA. This minimum resembles MCPA, but the three-membered ring is distorted in the plane (see Supporting Information for the structure called MCPA-distorted).
- (54) The orthogonal  $\pi$  orbitals in the triple bond of BTY give rise to two nearly degenerate electronic states of A' and A'' symmetry. The SCF procedures tend to converge to the A' state instead of to the A'' state, which is lower in energy at all levels (about 0.4 kcal/mol at UMP2).
- (55) Sastry, G. N.; unpublished results of B3LYP calculations.